

From single dots to interacting arrays

Vidar Gudmundsson^a Andrei Manolescu^{a,b} Roman Krahné^c
Detlef Heitmann^c

^a*Science Institute, University of Iceland, Dunhaga 3, IS-107 Reykjavik, Iceland*

^b*Institutul Național de Fizica Materialelor, C.P. MG-7 București-Măgurele,
România*

^c*Institut für Angewandte Physik und Zentrum für Mikrostrukturforschung,
Universität Hamburg, Jungiusstraße 11, D-20355 Hamburg, Germany*

Abstract

We explore the structural changes in charge the density and the electron configuration of quantum dots caused by the presence of other dots in an array, and the interaction of neighboring dots. We discuss what recent measurements and calculation of the far-infrared absorption reveal about almost isolated quantum dots and investigate some aspects of the complex transition from isolated dots to dots with strongly overlapping electron density. We also address the the effects on the magnetization of such dot array.

1 Introduction

Arrays of quantum dots of different shapes and sizes have been explored by far-infrared (FIR) absorption measurements and Raman scattering for a decade by many research groups. The main reason for using arrays has been the need to increase the signal strength of the tiny quantum dots in the weak radiation field applied, whose wavelength is up to 4 orders of magnitude larger than the dots. For lithographically prepared and etched quantum dots no evidence has been found for interaction between the dots on the length scale made available by laser holography for periodic structures. Recently, experiments on field-effect-confined quantum dots in $\text{Al}_x\text{Ga}_{1-x}/\text{GaAs}$ heterostructures have yielded signs that have been interpreted as being caused by the periodicity of the confinement potential of the array [1]. Evidence of direct interaction between dots in this same system have also been found [2]. Here we shall review these two cases together with the model calculations used for their interpretation. Such inter-dot interaction had so far only been observed for

adjacent large, 20-micron-size, 2D-electron disks in microwave experiments [3].

For the parameters available in field-effect-induced arrays of quantum dots with, typically, a lattice length of few hundred nanometers the interaction effects are expected to be small on the scale of the confinement energy $\hbar\Omega$. As this energy anyways lies in the range of few meV, where the low experimental sensitivity makes measurements challenging, it can be expected that mainly interaction effects leading to changes in the shape of the dots can be detected. With this in mind we explore numerically the subtle effects of the interaction on the ground state of elliptic dots in arrays with a bit shorter lattice length, than is now common in experiments. In addition, we consider the effects on the FIR absorption and the orbital magnetization of the dots. The magnetoplasmon excitations in arrays of circular and noncircular quantum dots have been studied by Zyl et al. in the Thomas-Fermi-Dirac-von Weizsäcker semiclassical approximation [4]. They study the deviations from the ideal collective excitations of isolated parabolically confined quantum dots caused by the local perturbation of the confining potential as well as the interdot Coulomb interaction and find the latter indeed to be unimportant unless the interdot separation is of the order of the size of the dots. An analytical model of parabolically confined electrons has been presented with a simplified inter-dot interaction. The model predicts shifts of collective modes and appearance of other modes that are not dipole active [5].

Commonly, experimental results on the FIR absorption of quantum dots in $\text{Al}_x\text{Ga}_{1-x}/\text{GaAs}$ heterostructure have successfully been interpreted in terms of a model of an isolated quantum dot with confinement potential that is parabolic or steeper. The pure parabolic confinement is caused by uniformly distributed ionized donors in the AlGaAs layer that have supplied their electrons to the active dot layer. Furthermore, the extension of the Kohn theorem explains why only center-of-mass modes can be excited in such dots with FIR radiation with wavelength much larger than the dot size [6–8]. Dots satisfying these criteria thus only show a single absorption peak at the frequency of the naked parabolic confinement. In magnetic field the peak splits into two peaks, one approaching the cyclotron frequency from above with increasing magnetic field strength B , and the other decreasing in frequency. The two collective modes are excited with FIR radiation with opposite circular polarization. In accordance with present possibilities in sample preparation, or dot design, the most common deviations from the simple circular parabolic confinement studied have been; elliptic dots, dots with weak square symmetry, and dots with quartic or stronger confinement. Elliptic shape of dots shows up as a simple splitting of the absorption peak at $B = 0$ [9,10], and the square shape produces a characteristic splitting in the upper Kohn mode at finite magnetic field [8,11]. The stronger confinement can produce a trivial blue shift and weaker absorption peaks with magnetic dispersion almost parallel to and above the

upper Kohn mode [12,13]. In addition, in confinement potentials that do not fulfill the criteria for the Kohn theorem so called Bernstein modes are excited causing characteristic splitting in the upper Kohn mode around higher harmonics of the cyclotron frequency [14,15]. Interestingly enough, researchers have been able to produce ring shaped quantum dots and measure their FIR absorption, but these do not form regular arrays [16–19].

2 Effects of an array

The simplest effects of an array of quantum dots on the confinement potential of an individual dot would be the eventual flattening of the potential imposed by the periodicity of the array. In field-induced dot arrays, where each dot contains only few electrons, it must be possible to have the confinement potential shallow enough that at least electrons in the excited states are affected by this weakening of the confinement. This has been demonstrated by Krahné et al. [1]. The experimental dispersion curves are seen in Fig. 1 for 6 or 30 electrons in each quantum dot. A purely parabolically confined quantum dot has the FIR dispersion of the Kohn modes

$$\omega_{\pm} = \sqrt{\Omega_0^2 + (\omega_c/2)^2} \pm \omega_c/2, \quad (1)$$

where Ω_0 is the confinement frequency, and $\omega_c = eB/(m^*c)$ is the cyclotron frequency. We have fitted this dispersion with the lower absorption branch and the sharper upper one in the experimental dispersion curves displayed in Fig. 1. In addition to these two branches the experiments show a third branch just below ω_+ however, above the cyclotron frequency ω_c .

It is well known that the energy spectrum of electrons in a periodic lattice can be calculated only for a magnetic flux commensurable with the unit cell [20]. It is technically difficult to vary the magnetic field continuously to describe the experimental results for an array of dots with interacting electrons [21,22]. We thus resort to a model of an individual quantum dot in the Hartree approximation, but with a potential of the form

$$V(x) = ax^2 + bx^4 + W(x), \quad (2)$$

where $x = r/a_0^*$ is the radial coordinate scaled by the effective Bohr radius $a_0^* = 9.77$ nm in GaAs and

$$W(x) = c[1 - f(3.9x - 12)], \quad (3)$$

with $f(x) = 1/(\exp(x) + 1)$. The calculated FIR absorption is shown in Fig. 2 for the parameter choice $a = 0.48$ meV, $b = -1.8^{-3}$ meV, and $c = 6$ meV. These parameters have been selected to give results qualitatively close to the experiment, without performing an actual fit. The model yields a mode just below ω_+ as is seen in the experiment. At low magnetic field the upper Kohn branch, ω_+ , has a complex splitting around $\omega = 2\omega_c$ that is dependent on the number of electrons present and for a higher number of electrons develops into a splitting caused by a Bernstein mode [14,15]. At high magnetic field the induced density of the ω_+ mode indeed reflects a center-of-mass mode, but the lower mode, the new one, is the lowest internal mode with one node in the center of the dot [1]. For a confinement stronger than the parabolic one (for example, with $b > 0$ and $c = 0$) this internal mode is usually found above the upper Kohn mode, but here due to the special confinement it has lower energy.

This is clearly an effect of the shape of the confinement potential of an individual quantum dot in an array, but what about a direct interaction between dots?

3 Interaction between dots

3.1 Experimental indications

Indications for interaction between quantum dots have been found in the same type of system when the dots have been prepared to have an elliptic symmetry rather than the circular one [2]. In elliptical quantum dots the rotational symmetry is broken and the degeneracy of the ω_+ and ω_- modes is lifted at $B = 0$. The dispersion of the FIR absorption peaks in a single elliptic quantum dot with parabolic confinement is described by

$$\omega_{\pm}^2 = \frac{1}{2} \left(\omega_x^2 + \omega_y^2 + \omega_c^2 \pm \sqrt{\omega_c^4 + 2\omega_c^2(\omega_x^2 + \omega_y^2) + (\omega_x^2 - \omega_y^2)^2} \right), \quad (4)$$

where ω_x and ω_y are, respectively, the resonance frequencies for the oscillation in the x and y direction at $B = 0$, the two symmetry axis of the dot. Let us consider the long axis of the ellipse to be aligned with the y axis of the coordinate system. The two modes $\omega_+(B = 0) = \omega_x$ and $\omega_-(B = 0) = \omega_y$ are observed with orthogonal linear polarization [2]. Figure 3 shows the magnetic dispersion of the absorption peaks for 3 different values of the gate voltages which is used to control the number of electrons in each quantum dot. For few electrons, Fig. 3(a), the dispersion with two peaks at $B = 0$ reflects the elliptic shape of the quantum dots. Curiously enough, for a higher number of

electrons, Fig. 3(b), the peaks at $B = 0$ are degenerate and the curves conform with the dispersion measured [11] and calculated [8] for square shape dots with a characteristic anticrossing in the ω_+ mode at a nonvanishing magnetic field. At even higher electron number, Fig. 3(c), the characteristic traits of the square shape are lost, no anticrossing at finite B and no degeneracy of the modes at $B = 0$ is discernible, but now the dispersion can be well fitted by the formula for elliptic dots (4) again. Linearly polarized measurements show that for all gate voltages the energetically higher excitation is polarized in x direction and the energetically lower in y direction. This shows that no rotation of the ellipse out of some electrostatic reason takes place. Thus the actual geometrical shape of the dots must be deformed by some interaction with their neighbors in dependence of the gate voltage.

3.2 Model results for interacting dots; Ground state properties

We model an array of quantum dots as interacting electrons in a periodic potential. We choose to describe the interaction of electrons within a dot at the same level as the interaction of electrons in different dots. In order to distinguish between the effects of different parts of the interaction, the direct one, the exchange, and correlation part, we use density functional theory (DFT) approach in the local spin density approximation (LSDA) to be described below. We describe a simple array of circular or elliptic dots (or antidots) shaped by the potential

$$V_{\text{QAD}}(\mathbf{r}) = V_0 \left[\sin\left(\frac{g_1 x}{2}\right) \sin\left(\frac{g_2 y}{2}\right) \right]^2, \quad (5)$$

where g_i is the length of the fundamental inverse lattice vectors, $\mathbf{g}_1 = 2\pi\hat{\mathbf{x}}/L_x$, and $\mathbf{g}_2 = 2\pi\hat{\mathbf{y}}/L_y$. The Bravais lattice defined by V_{QAD} has period lengths L_x , L_y , and the inverse lattice is spanned by $\mathbf{G} = G_1\mathbf{g}_1 + G_2\mathbf{g}_2$, with $G_1, G_2 \in \mathbf{Z}$. The commensurability condition between the magnetic length $\ell = (\hbar c/(eB))^{1/2}$ and the periods L_i requires magnetic-field values of the form $B = pq\phi_0/L_x L_y$, with $p, q \in \mathbf{N}$ flux quanta, $\phi_0 = hc/e$, in a unit cell [23,21]. Arbitrary rational values can, in principle, be obtained by resizing the unit cell in the Bravais lattice, but numerically this is quite difficult. The term 'circular quantum dot' can of course only describe a dot with few electrons in a square lattice where the electron density is concentrated in the middle of the cell and vanishes well before the cell edge. As the number of electrons increases the electron density must reflect the symmetry of the lattice. The dot potential (5) is seen in Fig. 4. We investigate different confinement potentials later on in order to understand better the interaction between dots. One of interest will be the simple

periodic cosine potential

$$V_{\text{per}}(\mathbf{r}) = V_0 \cos(g_1 x) + V_0 \cos(g_2 y), \quad (6)$$

shown in Fig. 5 for an array of elliptic dots.

The exchange-correlation energy per particle, $\epsilon_{xc}(\nu, \xi)$, is parameterized in terms of the total filling factor $\nu = \nu_\uparrow + \nu_\downarrow = 2\pi\ell^2 n$ and the spin polarization

$$\xi = \frac{\nu_\uparrow - \nu_\downarrow}{\nu_\uparrow + \nu_\downarrow} \quad (7)$$

rather than the spin densities n_\uparrow and n_\downarrow [24]. The exchange-correlation potentials are then

$$V_{xc\uparrow\downarrow} = \frac{\partial}{\partial\nu}(\nu\epsilon_{xc}) \pm (1 \mp \xi) \frac{\partial}{\partial\xi}\epsilon_{xc}, \quad (8)$$

and the exchange-correlation energy is interpolated as

$$\epsilon_{xc}(\nu, \xi) = \epsilon_{xc}^\infty(\nu)e^{-f(\nu)} + \epsilon_{xc}^{\text{TC}}(1 - e^{(1-f(\nu))}) \quad \text{with} \quad f(\nu) = 1.5\nu + 7\nu^4 \quad (9)$$

between the infinite magnetic field limit $\epsilon_{xc}^\infty = -0.782\sqrt{2\pi n}e^2/\kappa$ and the zero field limit $\epsilon_{xc}^{\text{TC}}$ given by Tanatar and Ceperly [25] generalized to intermediate polarizations [26].

In the numerical calculations we shall assume the magnetic flux density through the relevant unit cell to be constant and set to $B = 1.654$ T leading to a magnetic length $\ell = 19.95$ nm much smaller than the lattice lengths L_x and L_y , which shall be in the range 100 to 200 nm. It should be emphasized here that since the Coulomb interaction is treated equally for all electrons in the system, independent of whether they are in the same dot or not, we turn it totally off when we discuss a noninteracting system.

The resulting Kohn-Sham equations are solved within the symmetric Ferrari basis [27,23,21] and in order to have a large enough basis allowing several electrons in each dot we have to use lattice lengths L_i shorter than the actual ones in experiments. In the present calculations we use upto 16384 basis states. To get back to the experimental results displayed in Fig. 3 we perform a calculation for the ground state properties of an array of dots described by the confinement potential

$$V_{\text{sq}}(\mathbf{r}) = V_0 \left[\sin\left(\frac{g_1 x}{2}\right) \left\{ \sin\left(\frac{g_2 y}{2}\right) \right\}^2 \right]^2. \quad (10)$$

This choice defines a square unit cell, but within each cell the dot confinement is elliptic. The model results are shown as density contours in Fig. 6 for a growing number of electrons. For few electrons the shape of the dots is very close to circular, but with increasing electron number the dots become more elliptic. For still a higher number of electrons the Coulomb repulsion between the narrower edges (their ends) of neighboring dots causes their shape to become more square like. For $N = 20$, when their density clearly overlaps the central region acquires a circular or elliptic form again. Now, we can not maintain that this demonstrates what happens in an absorption experiment, but by a comparison to the noninteracting case we can clearly see that the Coulomb interaction has a strong influence on the the shape of the dots as the number of electrons is increased.

To learn more about these effects we want to compare the results to what happens in the different confinement potentials (5) and (6) introduced above. We start with elliptic dots described by V_{QAD} in eq. (5) in a rectangular lattice. Although the lattice does not have a square shaped unit cell as the one defined by V_{sq} , the distance between the quantum dots measured in the x or the y direction can be expected to be comparable. The density for the noninteracting case can be seen in Fig. 7 with the contours displayed in Fig. 8 with the real aspect ratio between the x and the y axis. Up to $N = 20$ there is only a weak overlapping of the electron density of neighboring cells, but certainly the shape of the dots changes with growing N , even in the absence of the electron-electron interaction. For low N their ellipticity increases as N grows, but for higher electron number the shape slowly approaches the symmetry of the lattice.

The electron density for the interacting case can be seen in Fig. 9 together with the contours in Fig. 10. In contrast to the noninteracting case the Coulomb repulsion is strong enough to push the electron density to already overlap considerably at $N = 12$ or even a bit lower. Interestingly, the repulsion forces the electrons to form wires in the direction of the longer axis (y axis) of the ellipses. This behavior is continued to much higher number of electrons as can be verified in Fig. 11, and it can be understood as governed by two facts. First, the repulsion between the dots along the longer edge is stronger than between the shorter edges of the dots. Second, the lower slope of the confinement potential in the y direction than in the x direction determines an asymmetric screening in the electron system. In this connection, it is also clear that the electronic density in the elliptic dots in the square lattice defined by V_{sq} had more space to 'broaden' the dots by occupying the space along the long edge between them than in this system.

This comparison opens the question of the role of the steepness of the confining potential itself. To tackle that question we have redone the calculations for the simple cosine potential V_{per} defined by eq. (6) with a variable strength V_0

but a constant number of electrons $N = 20$. The results for the noninteracting electrons is displayed in Fig. 12. When V_0 is small the overlapping of the electron density into neighboring cells is of the same order of magnitude in both directions, but for strong modulation V_0 the overlapping only takes place between the longer edges of the cell, i.e. modulated wires are formed in the y direction. The curious fact is that absolutely the *contrary* happens for the interacting system shown in Fig. 13, where the wires are formed in the x direction, which is the longer axis of the unit cell. Here several energy bands are occupied in the case of 20 electrons in a unit cell. The single-particle states with high energy are not well localized in the minimum of the potential in the middle of the cell and thus the wave functions of neighboring cells overlap where the distance is the shortest, here in the direction of the short axis L_y . With the interaction turned-on the repulsion in this direction is stronger and the system forms wires in the direction with the shorter interface with the neighboring cell.

The softer confinement potential V_{per} causes more drastic difference between the interacting and the noninteracting electron system, than the more realistic dot confinement V_{QAD} , at least more realistic at the lattice lengths and number of electrons considered here.

We have performed the calculations for quantum dots in arrays with $L_x = L_y$ to confirm that no direction for 'wire formation' is preferred in that case, and when $L_y = 1.5L_x$ we already have the wire formation in the preferred directions well developed. To test which parts of the dot interaction are important in influencing the shape we have repeated some of the calculations excluding the exchange and correlation interaction. For the lattice lengths, the electron number, and the confinement selected here the exchange and correlation plays a minor role. There is a fine structure in the density that depends on it, but the overall properties are caused by the direct interaction as could be expected.

3.3 FIR absorption in the model of interacting dots

Due to the large size of the mathematical set of basis functions used in the ground state calculation, in order to describe dots with several electrons and an array with not too short lattice lengths, we are not able to perform a calculation of the FIR absorption for the system with the parameters used above. Instead, we can describe the electrons in the Hartree approximation (HA) without spin and in a smaller lattice with $L_x = 100$ nm and $L_y = 150$ nm in a lower magnetic field strength $B = 1.10$ T.

The FIR absorption is calculated in a self-consistent linear response [22] ex-

citing the system with an external electric field of the type

$$\mathbf{E}_{ext}(\mathbf{r}, t) = -i\mathcal{E}_0 \frac{\mathbf{k} + \mathbf{G}}{|\mathbf{k} + \mathbf{G}|} \exp \{i(\mathbf{k} + \mathbf{G}) \cdot \mathbf{r} - i\omega t\}. \quad (11)$$

Here we do not restrict the dispersion relation for the external field, $\omega(\mathbf{k} + \mathbf{G})$, to that of a free propagating electromagnetic wave, but we allow for the more general situation in which the external field is produced as in a near-field spectroscopy or in a Raman scattering set-up. The power absorption is found from the Joule heating of the self-consistent electric field [28,12], $-\nabla\phi_{sc}$, with $\phi_{sc} = \phi_{ext} + \phi_{ind}$,

$$P(\mathbf{k} + \mathbf{G}, \omega) = -\frac{\omega}{4\pi} [|\mathbf{k} + \mathbf{G}| \phi_{sc}(\mathbf{k} + \mathbf{G}, \omega) \phi_{ext}^*(\mathbf{k} + \mathbf{G}, \omega)]. \quad (12)$$

The induced potential ϕ_{ind} is caused by the density variation $\delta n_s(\mathbf{r})$ due to ϕ_{sc} , which can then in turn be related to the external potential by the dielectric tensor

$$\sum_{\mathbf{G}'} \epsilon_{\mathbf{G}, \mathbf{G}'}(\mathbf{k}, \omega) \phi_{sc}(\mathbf{k} + \mathbf{G}', \omega) = \phi_{ext}(\mathbf{k} + \mathbf{G}, \omega). \quad (13)$$

The dielectric tensor, $\epsilon_{\mathbf{G}, \mathbf{G}'}(\mathbf{k}, \omega) = \delta_{\mathbf{G}, \mathbf{G}'} - \frac{2\pi e^2}{\kappa |\mathbf{k} + \mathbf{G}|} \chi_{\mathbf{G}, \mathbf{G}'}(\mathbf{k}, \omega)$, is determined by the susceptibility of the electron system,

$$\chi_{\mathbf{G}, \mathbf{G}'}(\mathbf{k}, \omega) = \frac{1}{(2\pi L)^2} \int d\theta \sum_{\alpha, \alpha'} f_{\alpha, \alpha'}^{\theta, \theta - \mathbf{k}L}(\hbar\omega) J_{\alpha, \alpha'}^{\theta, \theta - \mathbf{k}L - \mathbf{G}L}(\mathbf{k} + \mathbf{G}) \left(J_{\alpha, \alpha'}^{\theta, \theta - \mathbf{k}L - \mathbf{G}L}(\mathbf{k} + \mathbf{G}') \right)^*, \quad (14)$$

where \mathbf{k} is in the first Brillouin zone, $\tilde{\mathbf{k}} = (k_x L_x, k_y L_y)$ and $\tilde{\mathbf{G}} = (G_1 L_x, G_2 L_y)$, κ is the dielectric constant of the surrounding medium, $\theta = (\theta_1, \theta_2) \in \{[-\pi, \pi] \times [-\pi, \pi]\}$, and

$$f_{\alpha, \alpha'}^{\theta, \theta'}(\hbar\omega) = \left\{ \frac{f^0(\varepsilon_{\alpha, \theta}) - f^0(\varepsilon_{\alpha', \theta'})}{\hbar\omega + (\varepsilon_{\alpha, \theta} - \varepsilon_{\alpha', \theta'}) + i\hbar\eta} \right\}, \quad (15)$$

in which f^0 is the equilibrium Fermi distribution, $\eta \rightarrow 0^+$, and

$$J_{\alpha, \alpha'}^{\theta, \theta'}(\mathbf{k}) = (\alpha'(\theta') | e^{-i\mathbf{k} \cdot \mathbf{r}} | \alpha(\theta)). \quad (16)$$

Special care must be taken with respect to the symmetry of the wave functions corresponding to the Hartree states $|\alpha(\theta)\rangle$ when translating them across the boundaries of the quasi-Brillouin zones.

In Fig. 14 we see the absorption for an array of electrons with two electrons in each dot (upper right panel) and an array of seven electrons (lower right panel). In the former case the dots are isolated, but in the latter case their densities start to overlap in the x and y directions, almost of the same amount. The structure of the corresponding energy bands is displayed in the left panels of Fig. 14, showing that, indeed, when 7 electrons occupy each dot the chemical potential μ is situated in the continuum states. We fix the polarization of the external field (11) by giving \mathbf{k} a small but finite value, $\mathbf{k}_i L_i = 0.2$ with $i = x, y$, and $\mathbf{G} = 0$ in accordance with FIR radiation. The FIR absorption of the isolated dots consists of two peaks, one sharp peak and the second broadened and lower. Since the confinement is not parabolic there are higher order peaks at still higher energy that we exclude from our discussion and figure here. At the higher electron number we still can locate the two main peaks, now both split. At an energy below the collective dot modes, which are not dependent on the direction of \mathbf{k} , we find intraband modes caused by transitions in the Landau band where the chemical potential is located. These intraband modes depend on the direction of \mathbf{k} as the structure of the low lying continuum bands reflects the geometry of the dot array. They are generally not seen in experimental spectra since for larger lattice lengths they are at a very low energy range that is not easily accessible.

As we can only consider a very limited system here, we have to be careful about generalizations, but if we analyze the gap between the sets of peaks as a function of the electron number N in the range between 2 and 12 electrons we can see a tendency to a similar evolution as has been reported in experiment [2] and is repeated in Fig. 3. This should only be considered as a very preliminary result and one has to keep in mind that we perform our calculation at a finite magnetic field since the calculation is built on a basis set which has to increase when the magnetic field decreases.

3.4 *Effects on magnetization in the ground state*

Recently, our attention has been drawn to measurements of the magnetization of a homogeneous two-dimensional electron gas (2DEG) in heterostructures [29,30]. There are efforts underway to extend the experiments on magnetization also to modulated 2DEG's and arrays of dots and antidots. The magnetization is an equilibrium property of the ground state of the electron system so we can calculate it for the system in which we have studied the shape changes of the quantum dots as function of the number of electrons N . The total magnetization can be calculated according to the definition for the orbital M_o and

the spin component of the magnetization M_s , [31,32]

$$M_o + M_s = \frac{1}{2c\mathcal{A}} \int_{\mathcal{A}} d^2r (\mathbf{r} \times \langle \mathbf{J}(\mathbf{r}) \rangle) \cdot \hat{\mathbf{n}} - \frac{g\mu_B}{\mathcal{A}} \int_{\mathcal{A}} d^2r \langle \sigma_z(\mathbf{r}) \rangle, \quad (17)$$

where \mathcal{A} is the total area of the system. The equilibrium local current is evaluated as the quantum thermal average of the current operator,

$$\hat{\mathbf{J}} = -\frac{e}{2} \left(\hat{\mathbf{v}}|\mathbf{r}\rangle\langle\mathbf{r}| + |\mathbf{r}\rangle\langle\mathbf{r}|\hat{\mathbf{v}} \right), \quad (18)$$

with the velocity operator $\hat{\mathbf{v}} = [\hat{\mathbf{p}} + (e/c)\mathbf{A}(\mathbf{r})]/m^*$, \mathbf{A} being the vector potential.

A typical current density is shown in Fig. 15 superimposed on the contours of the electron density for one elliptical quantum dot in an array of dots. Even though the density has only one maximum two vortices are seen in the current density. Here again we have used the LSDA described above. The orbital magnetization of arrays of elliptical dots and antidots of different aspect ratio is presented in Fig. 16 and for comparison the last panel shows the magnetization for the electronic system confined by V_{per} (6). The magnetization for the antidot array is almost simply the mirror image of the magnetization for the dot array for the range of N considered here, independent of whether the system forms isolated dots or not. For low N the M_o develops peaks when N equals twice the number of flux quanta pq through the unit cell, i.e. when only the lowest Landau band is completely occupied and all other bands are empty. The spin contribution to the magnetization, M_s , seen in the left panel of Fig. 17, reflects strong spin polarization as $N = pq$, when the first Landau band is half filled and the exchange energy is thus enhanced. This enhancement of the exchange can also be recognized at higher odd integer multiples of pq .

The situation is a bit different for the electron system confined or modulated by V_{per} (6). Here the splitting of the Landau bands into Hofstadter bands [20,23,21] is stronger than the exchange enhancement of the spin splitting reflected by the fact that the spin contribution to the magnetization M_s in the right panel of Fig. 17 vanishes for even number of electrons in most cases and no strong spin polarization is observed. This happens even when the iteration process of the LSDA has been started with an artificial large g factor that is later reduced to the natural value of 0.44 appropriate for GaAs. The last panel of Fig. 16 shows that the orbital magnetization M_o is also quite different for this system: First, its magnitude does not increase as drastically with the size of the unit cell as for the dots and antidots. Second, the Hofstadter splitting in the lowest Landau band when it is half filled produces a clearer signature than the complete filling of the band. The difference in the magnetization for these two systems has to be connected to their different geometry. At low N

the confinement V_{QAD} produces simple dots or antidots, the dots are isolated at first but start to overlap only after the first Landau band has been fully occupied. On the other hand, the electron system in V_{per} forms connected regions for lower N . At this moment we have not discovered any clear signs of the actual geometry of the dots and antidots in the magnetization, and thus we can not distinguish the magnetization of circular or elliptic quantum dots. In order to accomplish this in isolated dots with few electrons we would need to be able to vary the magnetic field continuously for a constant number of electrons [33].

4 Summary

We have reported here on efforts to discern in experiments or predict by model calculations the effects arrays can have on the FIR absorption of quantum dots. There are indications that effects of the periodicity itself have been detected in measured FIR spectra, and even interaction between neighboring quantum dots. Model calculations confirm that the effects of the periodicity are well understood, but the effects of a direct interaction between the electron systems of different dots is very weak and subtle. The direct interaction though seems to be detectable if it can influence the shape of the dots, since the FIR absorption is very dependent on the symmetry of the electron system confined in them.

Acknowledgments

We gratefully acknowledge support from the German Science Foundation DFG through SFB 508 “Quanten-Materialien”, the Graduiertenkolleg “Nanostrukturierte Festkörper”, the Research Fund of the University of Iceland, and the Icelandic Natural Science Council. We thankfully acknowledge the great help of Birgir F. Erlendsson in parallelizing the execution of the core regions of our programs.

References

- [1] R. Krahne, V. Gudmundsson, C. Heyn, and D. Heitmann, Phys. Rev. B **63**, 195303 (2001).
- [2] R. Krahne, V. Gudmundsson, C. Heyn, and D. Heitmann, Physica E p. in print (2001).

- [3] C. Dahl and J. P. Kotthaus, Phys. Rev. B **46**, 15590 (1992).
- [4] B. P. van Zyl, E. Zaremba, and D. A. W. Hutchinson, Phys. Rev. B **61**, 2107 (2000).
- [5] M. Taut, Phys. Rev. B **62**, 8126 (2000).
- [6] P. A. Maksym and T. Chakraborty, Phys. Rev. Lett **65**, 108 (1990).
- [7] D. A. Broido, K. Kempa, and P. Bakshi, Phys. Rev. B **42**(17), 11400 (1990).
- [8] D. Pfannkuche and R. Gerhardtts, Phys. Rev. B **44**(23), 13132 (1991).
- [9] S. K. Yip, Phys. Rev. B **43**, 1707 (1991).
- [10] Q. P. Li, K. Karraï, S. K. Yip, S. D. Sarma, and H. D. Drew, Phys. Rev. B **43**(6), 5151 (1991).
- [11] T. Demel, D. Heitman, P. Grambow, and K. Ploog, Phys. Rev. Lett. **64**, 788 (1990).
- [12] V. Gudmundsson and R. Gerhardtts, Phys. Rev. B **43**(14), 12098 (1991).
- [13] Z. L. Ye and E. Zaremba, Phys. Rev. B **50**(23), 17217 (1994).
- [14] V. Gudmundsson, A. Brataas, P. Grambow, T. Kurth, and D. Heitmann, Phys. Rev. B **51**, 17744 (1995).
- [15] I. B. Bernstein, Phys. Rev. **109**(1), 10 (1958).
- [16] A. Lorke, R. J. Luyken, A. O. Govorov, J. P. Kotthaus, J. M. Garcia, and P. M. Petroff, Phys. Rev. Lett. **84**, 2223 (2000).
- [17] E. Zaremba, Phys. Rev. B **53**(16), R10512 (1996).
- [18] J. M. Llorens, C. Trallero-Giner, A. Garca-Cristbal, and A. Cantarero, Phys. Rev. B **64**, 035309 (2001).
- [19] A. Emperador, M. Barranco, E. Lipparini, M. Pi, and L. Serra, Phys. Rev. B **62**(23), 4573 (2000).
- [20] R. D. Hofstadter, Phys. Rev. B **14**, 2239 (1976).
- [21] V. Gudmundsson and R. R. Gerhardtts, Phys. Rev. B **52**, 16744 (1995).
- [22] V. Gudmundsson and R. R. Gerhardtts, Phys. Rev. B **54**, 5223R (1996).
- [23] H. Silberbauer, J. Phys. C **4**, 7355 (1992).
- [24] M. I. Lubin, O. Heinonen, and M. D. Johnson, Phys. Rev. B **56**, 10373 (1997).
- [25] B. Tanatar and D. M. Ceperley, Phys. Rev. B **39**, 5005 (1989).
- [26] M. Koskinen, M. Manninen, and S. M. Reimann, Phys. Rev. Lett. **79**, 1389 (1997).
- [27] R. Ferrari, Phys. Rev. B **42**, 4598 (1990).

- [28] C. Dahl, Phys. Rev. B **41**(9), 5763 (1990).
- [29] I. Meinel, T. Hengstmann, D. Grundler, and D. Heitmann, Physical Review Letters **82**(4), 819 (1999).
- [30] I. Meinel, D. Grundler, D. Heitmann, A. Manolescu, V. Gudmundsson, W. Wegscheider, and M. Bichler, Phys. Rev. B **64**, 121306(R) (2001).
- [31] J. Desbois, S. Ouvry, and C. Texier, Nucl. Phys. B **528**, 727 (1998).
- [32] V. Gudmundsson, S. I. Erlingsson, and A. Manolescu, Phys. Rev. B **61**, 4835 (2000).
- [33] I. Magnúsdóttir and V. Gudmundsson, Phys. Rev. B **61**, 10229 (2000).

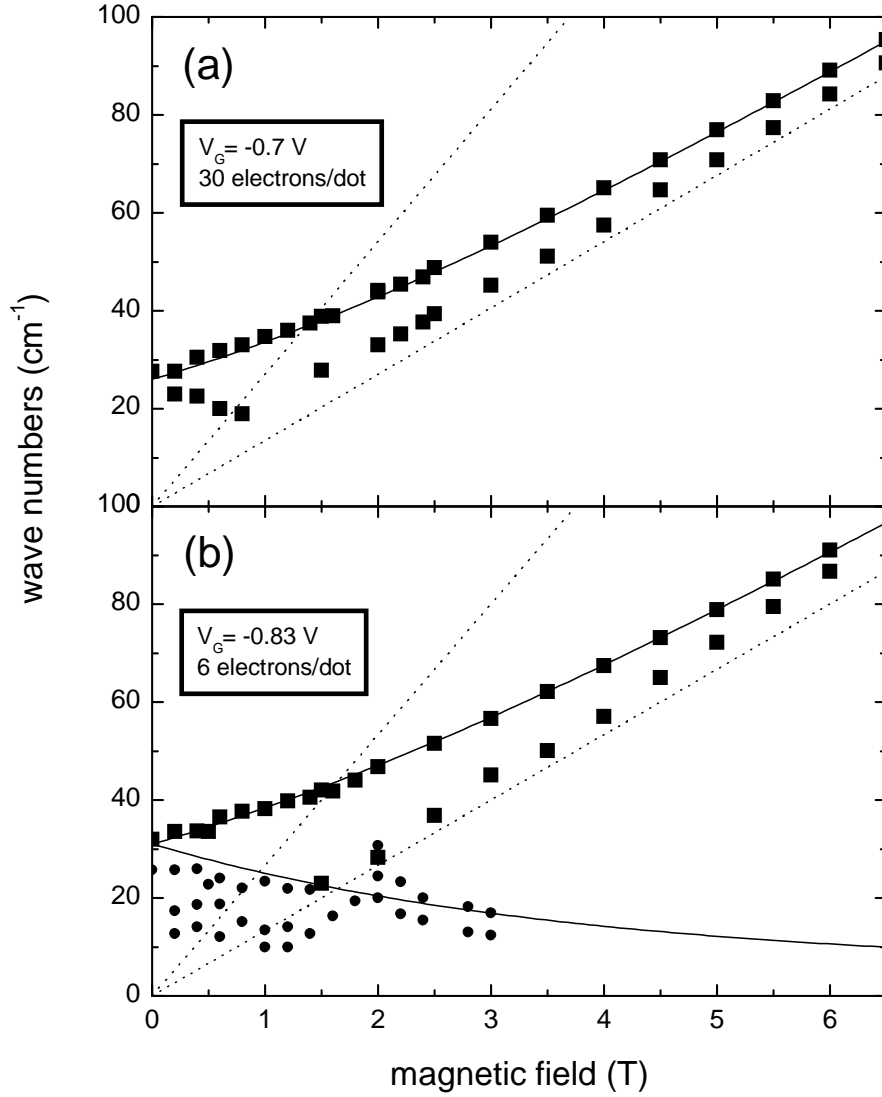


Fig. 1. Experimental dispersion for quantum dots with (a) 30 electrons and (b) 6 electrons. Full lines are fits with the Kohn modes of eq.(1), the dotted lines are ω_c and $2\omega_c$ extracted from this fit. A new mode, the below-Kohn mode, is observed *below* the upper Kohn mode but clearly *above* ω_c .

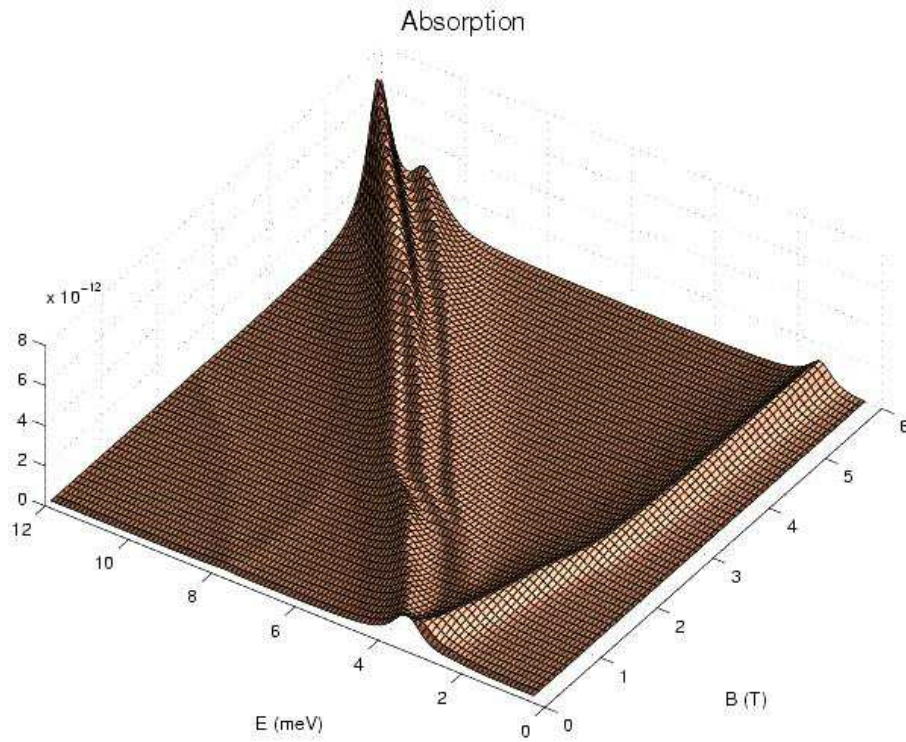


Fig. 2. Calculated dipole absorption for a quantum dot with 5 electrons in a flattened potential described in the text. In addition to the strong Kohn modes new modes below the high-frequency Kohn mode are found also in the calculation. The half-linewidth is 0.3 meV and $T = 1$ K.

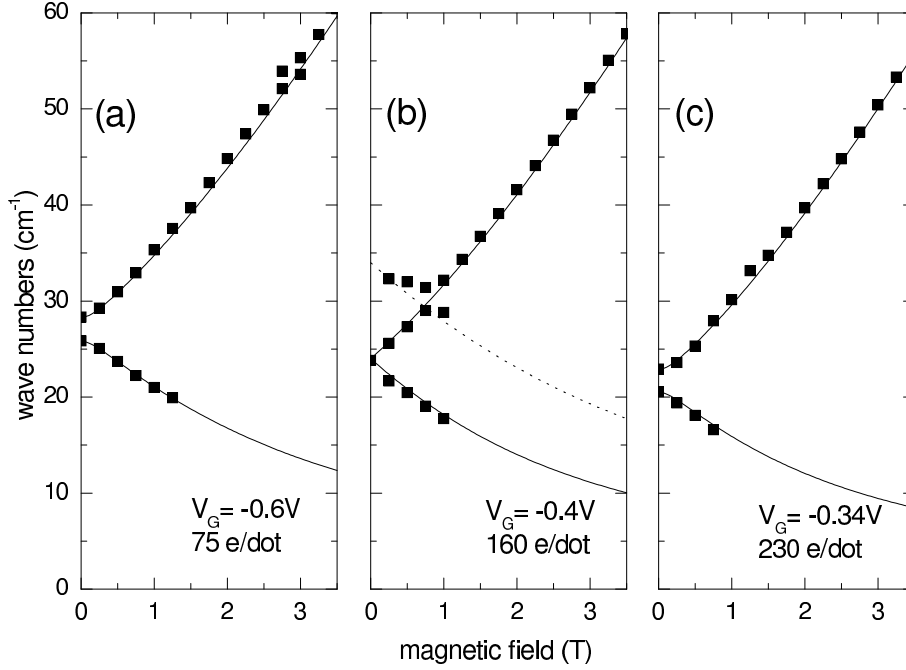


Fig. 3. Magnetic field dispersions for three different gate voltages. The experimental resonance positions extracted from the spectra are depicted by the full squares. The solid lines show a calculation according to eq. (4) with $\omega_{x(y)}$ as fit parameters. (a) $V_G = -0.6$ V: strong confinement leading to isolated dots. (b) $V_G = -0.4$ V: weaker confinement. Here an anticrossing of the ω_+ mode around $B = 1$ T with another weak resonance, which decreases in energy with increasing B , is observed. This anticrossing is behavior is a characteristic property of square symmetric quantum dots [11]. (c) $V_G = -0.34$ V: weak confinement leading to overlapping dots.

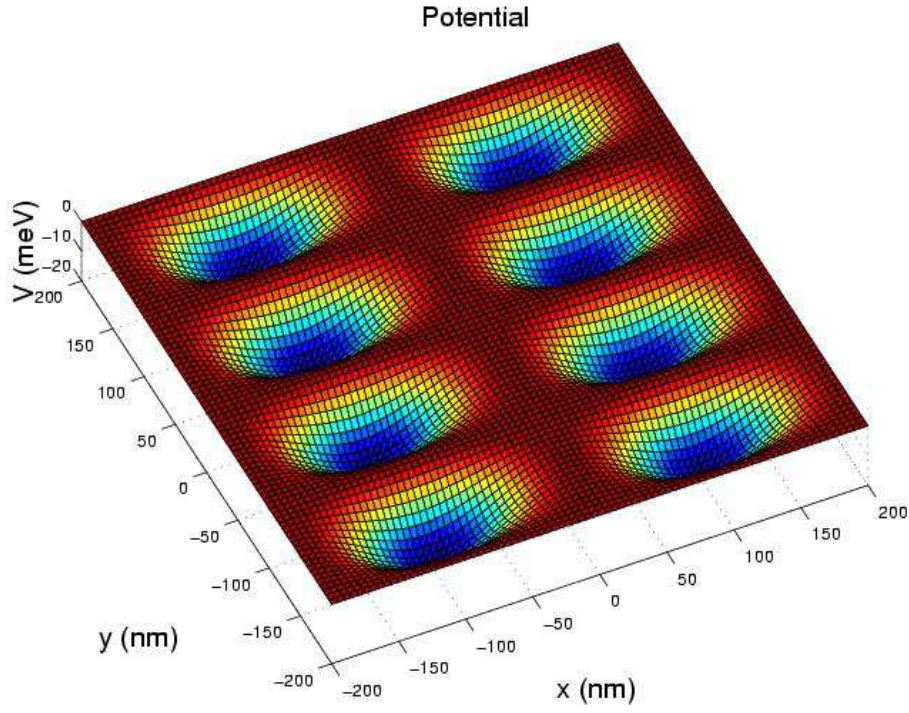


Fig. 4. The periodic confinement potential V_{QAD} for a dot array with aspect ratio 1:2. See equation (5) in text.

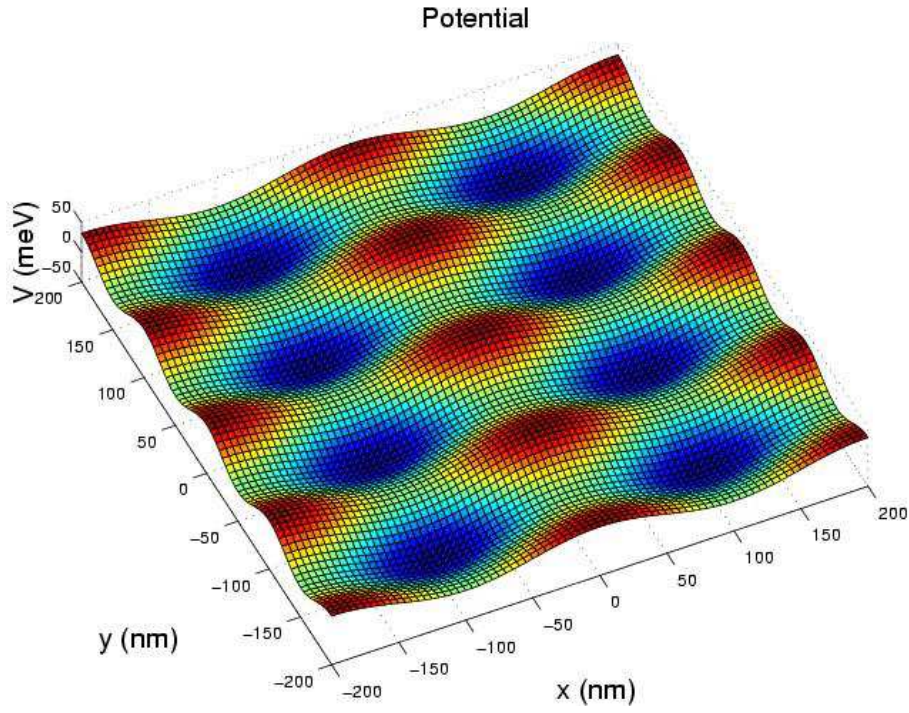


Fig. 5. The simple cosine confinement potential V_{per} with aspect ratio 1:2. See equation (6) in text.

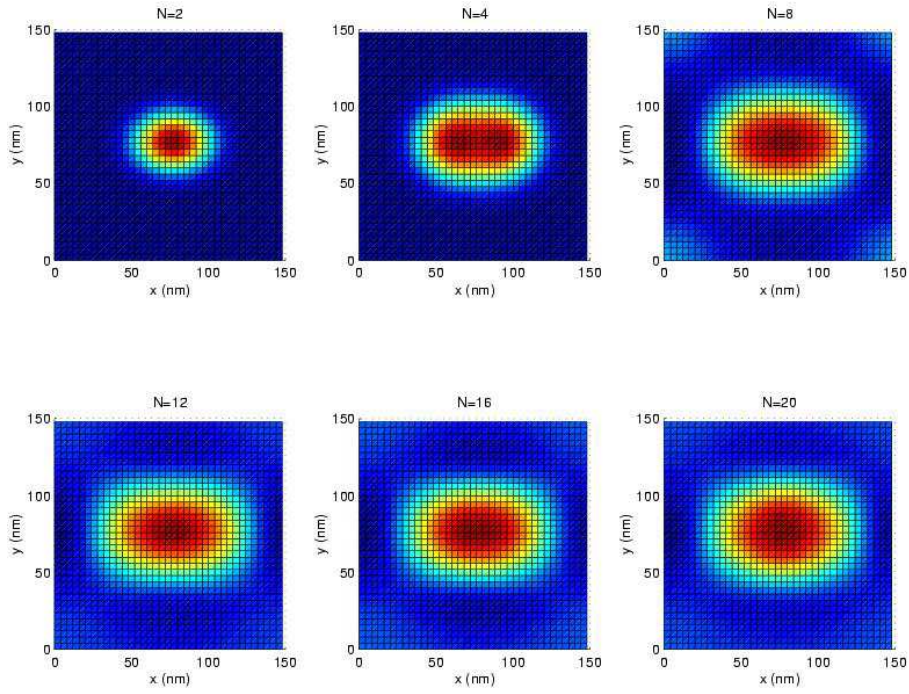


Fig. 6. The electron density distribution for the ground state of interacting elliptical dots in a square lattice. The confinement is according to eq. (10). $B = 1.654$ T, $T = 1$ K, $V_0 = -16$ meV.

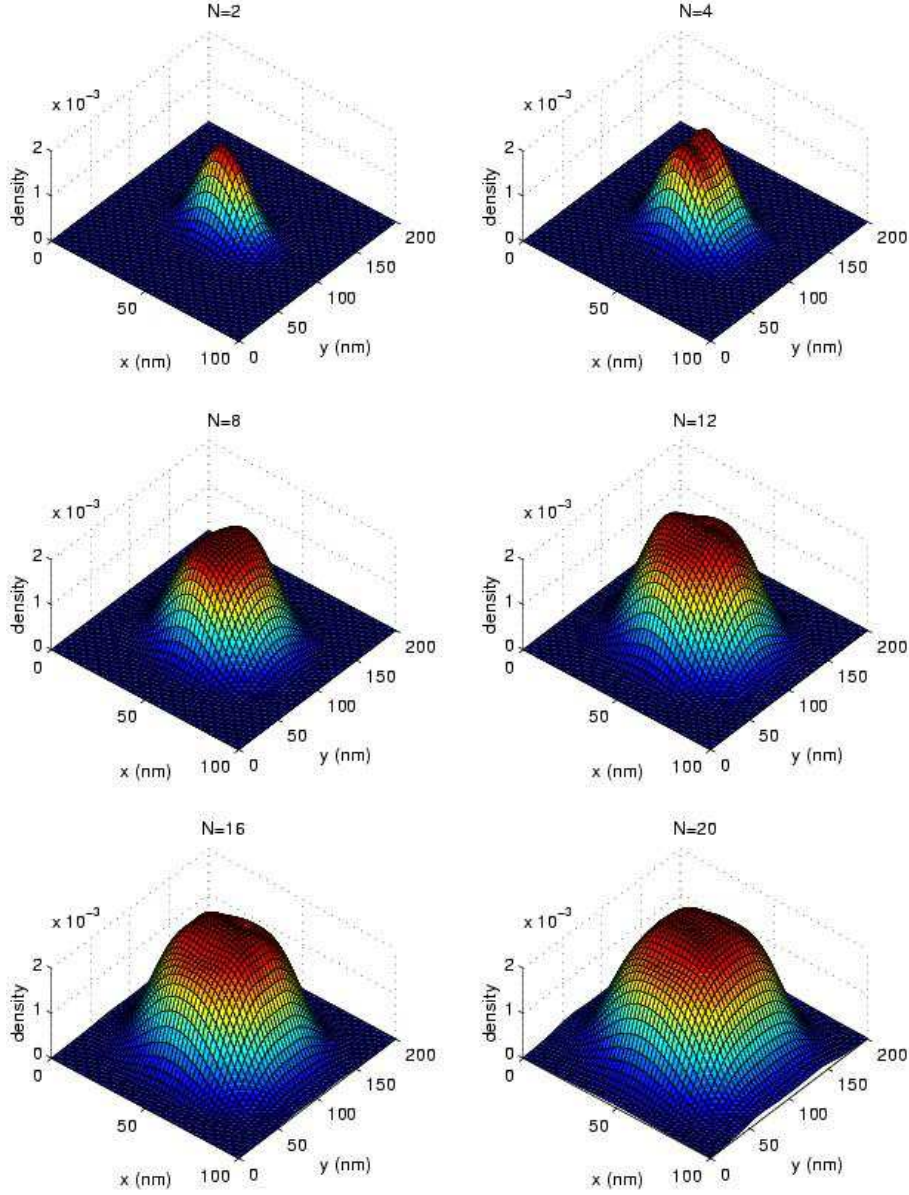


Fig. 7. The electron density distribution for the ground state of *noninteracting* elliptical dots. The confinement is according to eq. (5). The x and y axis are scaled differently here. $B = 1.654$ T, $T = 1$ K, $V_0 = -16$ meV.

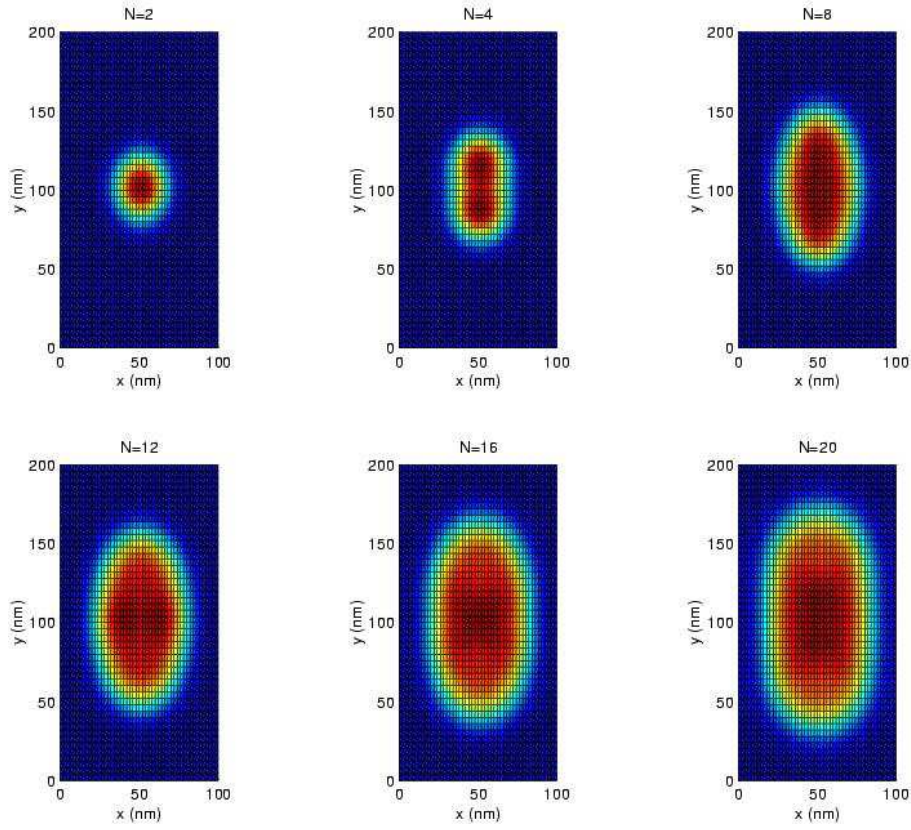


Fig. 8. The electron density distribution for the ground state of *noninteracting* elliptical dots. The confinement is according to eq. (5). Same case as in Fig. 7. $B = 1.654$ T, $T = 1$ K, $V_0 = -16$ meV.

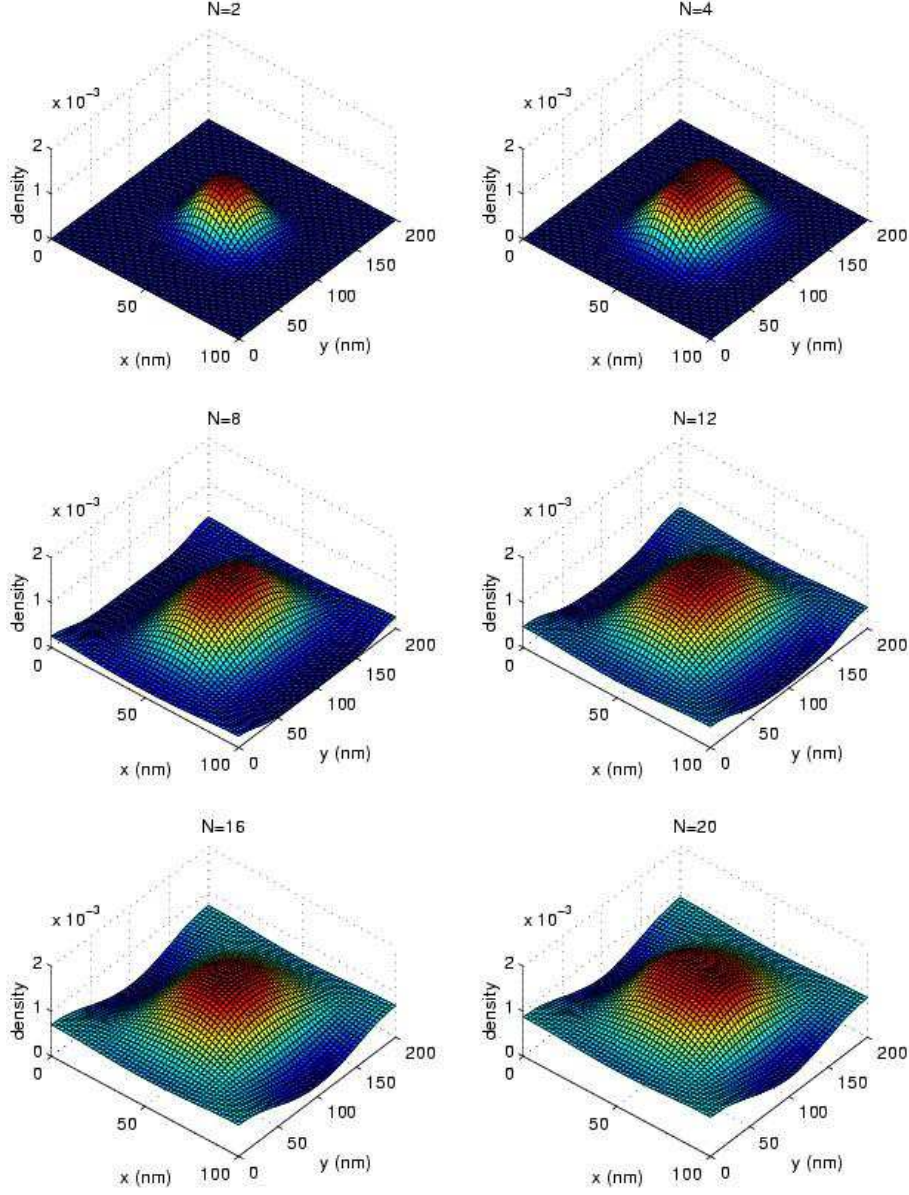


Fig. 9. The electron density distribution for the ground state of *interacting* elliptical dots. The confinement is according to eq. (5). The x and y axis are scaled differently here. $B = 1.654$ T, $T = 1$ K, $V_0 = -16$ meV.

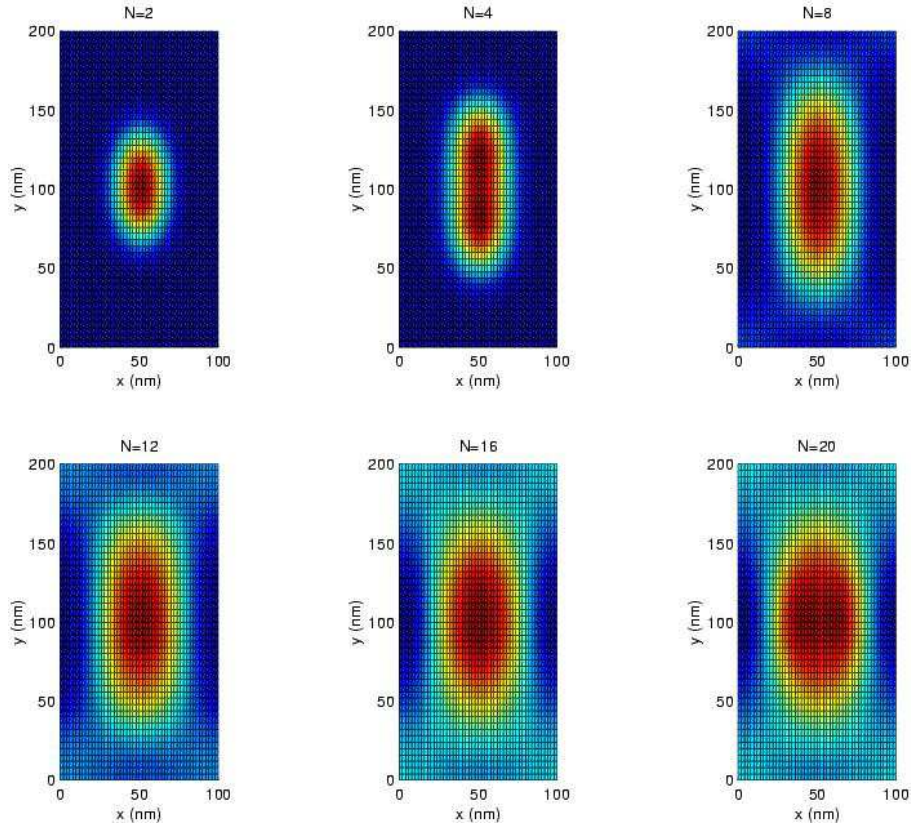


Fig. 10. The electron density distribution for the ground state of *noninteracting* elliptical dots. The confinement is according to eq. (5). Same case as in Fig. 9. $B = 1.654$ T, $T = 1$ K, $V_0 = -16$ meV.

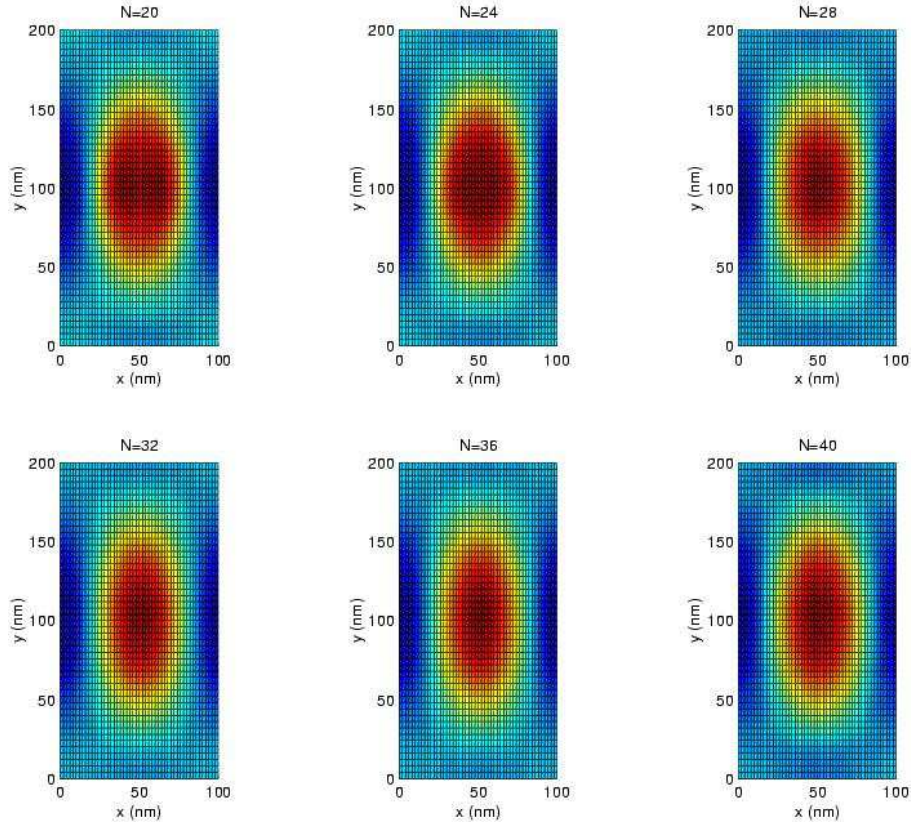


Fig. 11. The electron density distribution for the ground state of *noninteracting* elliptical dots. The confinement is according to eq. (5). Same system as in Fig. 10, but with a higher number of electrons. $B = 1.654$ T, $T = 1$ K, $V_0 = -16$ meV.

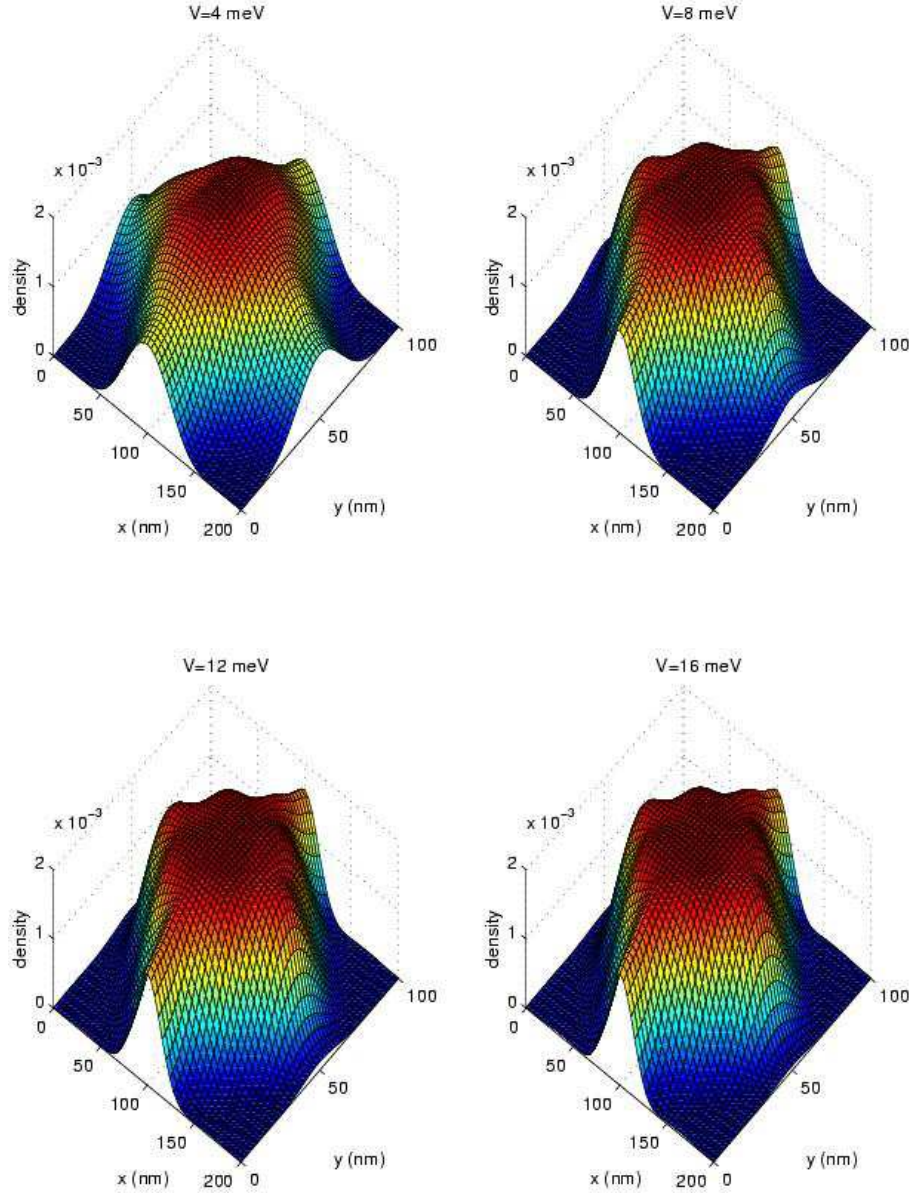


Fig. 12. The electron density distribution for the ground state of a *noninteracting* 2DEG in the simple periodic potential V_{per} described by eq. (5). The x and y axis are scaled differently here. $B = 1.654 \text{ T}$, $T = 1 \text{ K}$, $N = 20$.

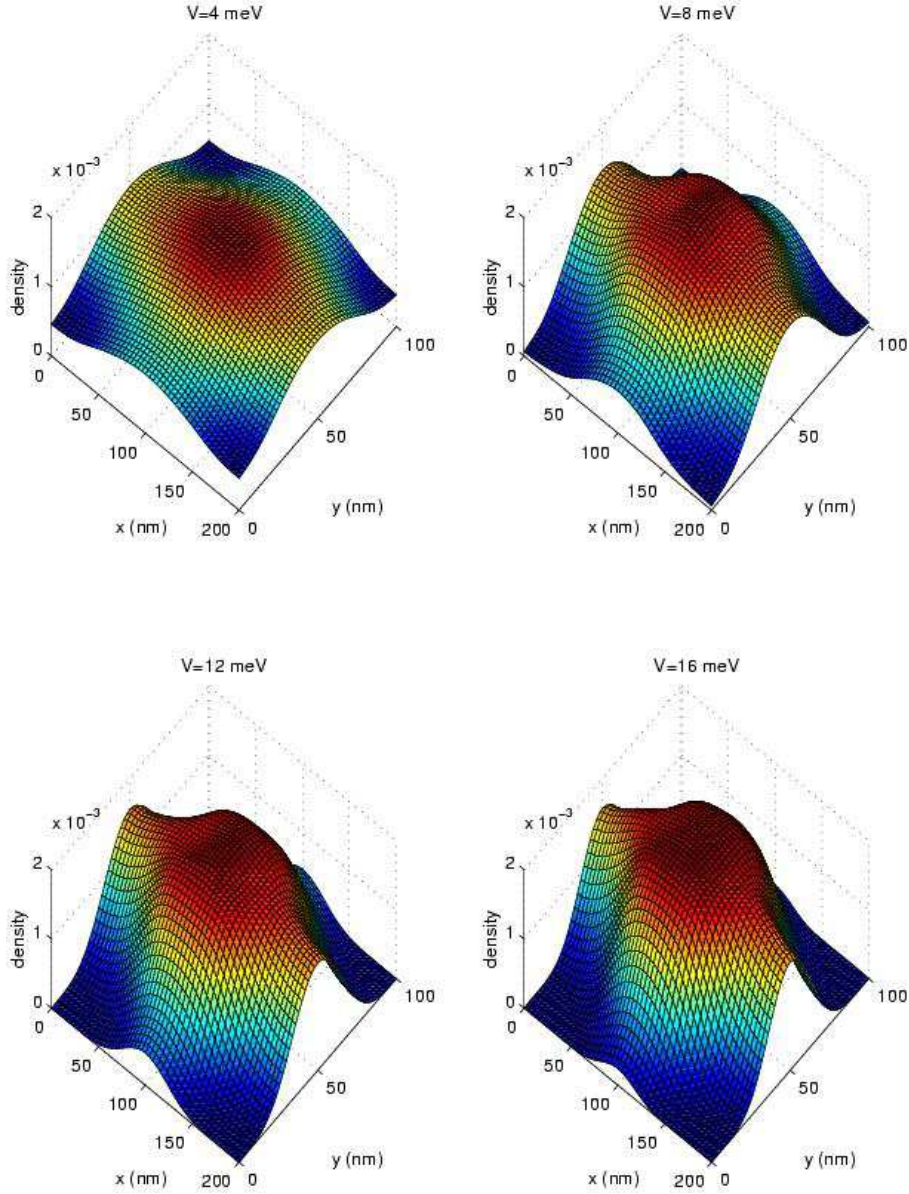


Fig. 13. The electron density distribution for the ground state of an *interacting* 2DEG in the simple periodic potential V_{per} described by eq. (5). The x and y axis are scaled differently here. $B = 1.654$ T, $T = 1$ K, $N = 20$.

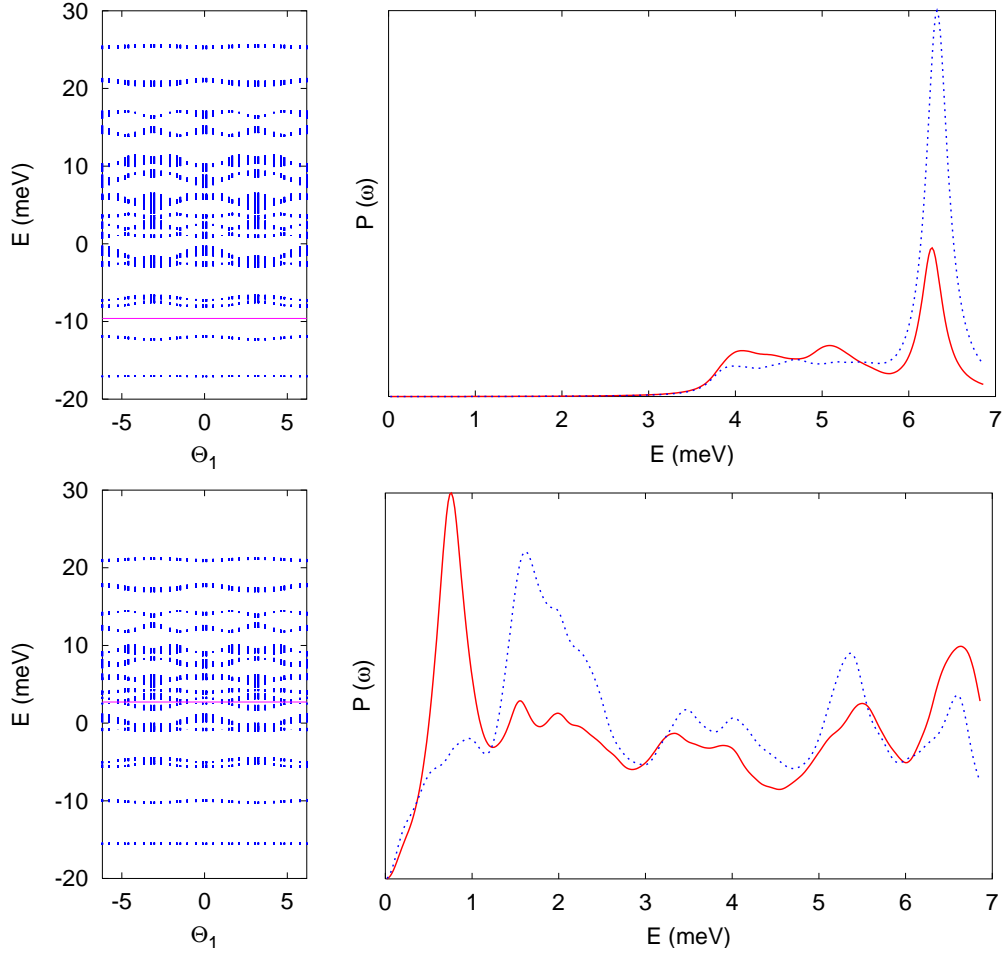


Fig. 14. The FIR absorption for two (upper panel) and seven electrons (lower panel) in the hartree approximation for spinless electrons. $k_x L_x = 0.2$ (solid curve), and $k_y L_y = 0.2$ (dotted curve). The right panels show the band structure projected on the $\Theta_1 = k_x L_x$ axis in the Brillouin zone. The chemical potential μ is indicated by the horizontal solid line.

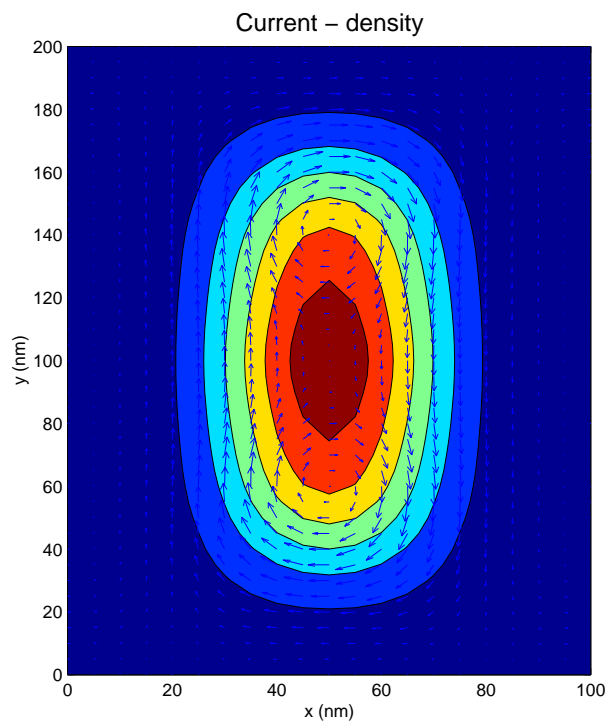


Fig. 15. The interacting electron and current density for 6 electrons in an elliptic quantum dot in the array described by eq. (5). $B = 1.654$ T, $T = 1$ K, $V_0 = -16$ meV.

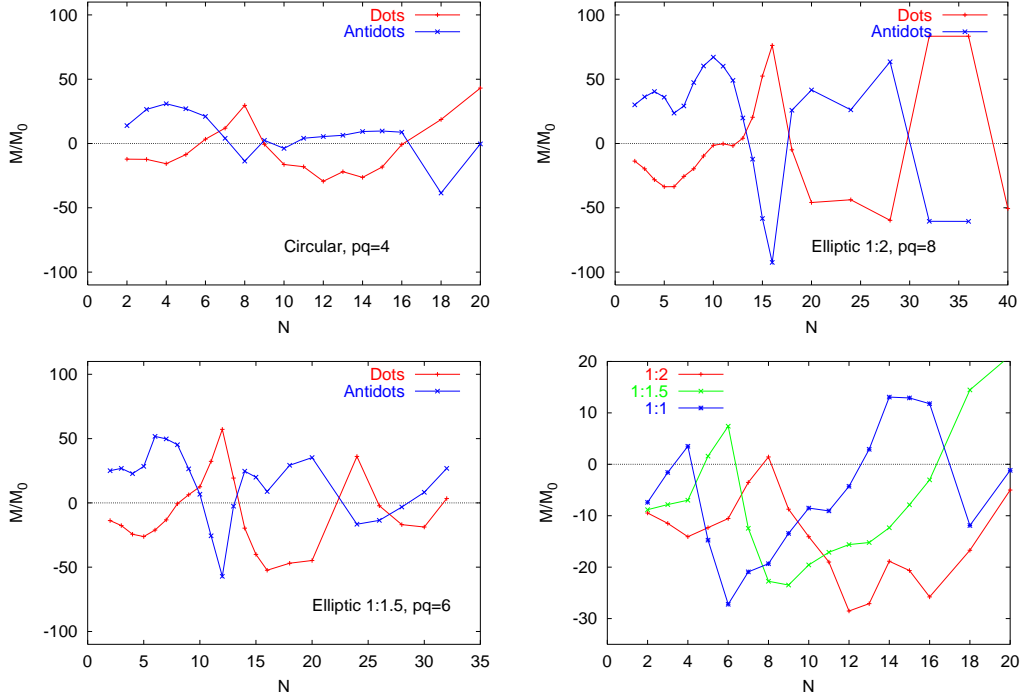


Fig. 16. The orbital magnetization M_o as function of the number of electrons N in a quantum dot or antidot array described by eq. (5) with aspect ratios 1:1 (upper left panel), 1:1.5 (upper right), 1:2 (lower left), a 2DEG confined by eq. (6) for all three aspect ratios (lower right panel). $M_0 = \mu_B^*/(L_x L_y)$, $B = 1.654$ T, $T = 1$ K, $|V_0| = 16$ meV.

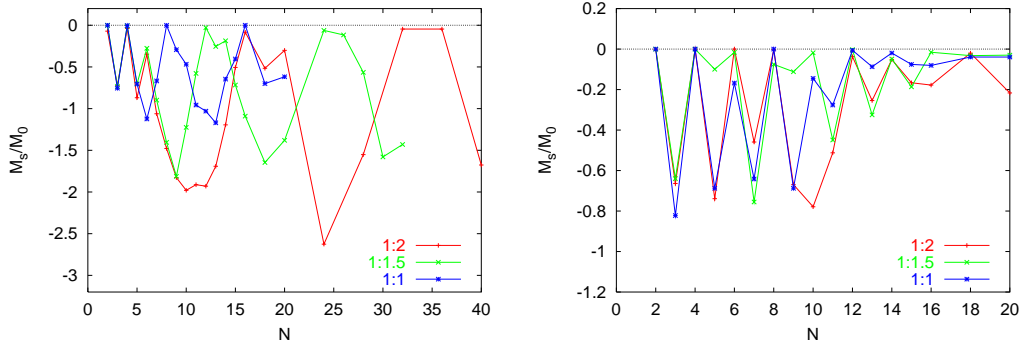


Fig. 17. The spin contribution to the magnetization M_s as a function of the number of electrons N for a dot array described by eq. (5) (left), and a 2DEG described by eq. (6). $M_0 = \mu_B^*/(L_x L_y)$, $B = 1.654$ T, $T = 1$ K, $|V_0| = 16$ meV.